

Topological quantum compilation of metaplectic anyons based on the genetic optimized algorithms

Jiangwei Long,¹ Jianxin Zhong,^{2,3,*} and Lijun Meng^{1,3,†}

¹*School of Physics and Optoelectronics, Xiangtan University,
Xiangtan 411105, Hunan, People's Republic of China.*

²*Center for Quantum Science and Technology, Department of Physics,
Shanghai University, Shanghai 200444, People's Republic of China.*

³*Hunan Key Laboratory for Micro-Nano Energy Materials and Devices, Hunan, People's Republic of China.*

(Dated: January 28, 2025)

Topological quantum computing holding global anti-interference ability is realized by braiding some anyons, such as well-known Fibonacci anyons. Here, based on $SO(3)_2$ theory we obtain a total of 6 anyon models utilizing F -matrices, R -symbols, and fusion rules of metaplectic anyon. We obtain the elementary braided matrices (EBMs) by means of unconventional encoding. After braid X and X' , we insert a pair of Z anyons into them to ensure that the initial order of anyons remains unchanged. In this process only fusion is required, and measurement is not necessary. Three of them $\{V_3^{113}, V_3^{131}, V_1^{133}\}$ are studied in detail. We study systematically the compilation of these three models through EBMs obtained analytically. For one-qubit case, the classical H - and T -gate can be well constructed using the genetic algorithm enhanced Solovay-Kitaev algorithm (GA-enhanced SKA) by $\{V_3^{113}, V_3^{131}, V_1^{133}\}$. The obtained accuracy of the H/T -gate by $\{V_3^{113}, V_1^{133}\}$ is slightly inferior to the corresponding gates of the Fibonacci anyon model, but it also can meet the requirements of fault-tolerant quantum computing, V_3^{131} giving the best performance of these four models. For the two-qubit case, we use the exhaustive method for short lengths and the GA for long lengths to obtain braidword for $\{V_3^{113}, V_3^{131}, V_1^{133}\}$ models. The resulting matrices can well approximate the local equivalence class of the CNOT-gate, while demonstrating a much smaller error than the Fibonacci model, especially for the V_3^{113} .

I. INTRODUCTION

The anyon is a quasi-particle excitation that exists in a two-dimensional plane, and the exchange of two anyons will result in a nontrivial phase, which was first proposed by Myrheim and Leinaas [1] in 1977. In 1997, Kitaev proposed that the use of anyons is expected to realize topological quantum computing for the first time [2]. The advantage of topological quantum computing is that information is stored globally and is not affected by local noise, so topological quantum computing is naturally robust. Topological quantum computing relies on the braiding of non-Abelian anyons [3–5]. Notable non-Abelian anyons include the Ising and Fibonacci anyons. Ising anyon can easily construct H -gate and CNOT-gate but cannot build T -gate [6–10]. Non-Abelian Fibonacci anyon can be used for universal quantum computing by braiding alone and has been discussed extensively in the past decades [11]. The standard H/T -gate cannot be directly constructed by Fibonacci anyon, and continuous braid operations are needed to ensure a sufficiently low error with a standard qubit gate. This sequence is called a braidword, which consists of some EBMs. As the length of the braidword increases, the search space will increase exponentially. Exhaustive search will quickly become infeasible due to high computational cost. How to find the best approximation between braidword and standard gate in an exponentially large space forms the

quantum compilation problem. Many methods have been proposed for the quantum compilation problem of the Fibonacci anyon model. Including hash function techniques [12], SKA [13], Monte Carlo enhanced SKA [14], machine learning [15], and GA [16]. For the construction of two-qubit gate using Fibonacci anyon, L. Hormozi et al. proposed the injection braid method [17], Haitan Xu proposed functional braid to construct CNOT-gates with low leakage error [18], two-qubit EBMs based on Fibonacci model are given by Cui et al. [19] and Phillip C. Burke et al. recently used these EBMs to construct a local equivalence class with CNOT-gate [20]. Fibonacci anyon was also used to construct a three-qubit gate, which was theoretically realized by Abdellah Tounsi et al. using an injection braid [21].

Although Fibonacci anyon can be used to realize universal quantum computing by braid alone, such anyon seems to be difficult to capture experimentally. A more easily implementable class of anyons for universal quantum computing is called weak integral anyon (corresponding to the quantum dimension $d^2 \in \mathbb{Z}$) [22], and weak integral anyon with F -property [23] includes metaplectic anyons [24–26]. Metaplectic anyons model $SO(p)_2$, when $p=3$, is equivalent to $SU(2)_4$, the anyons in the $SO(3)_2$ are expected to exist in fractional quantum Hall liquids with $v = 8/3$ [27], bilayer fractional quantum Hall liquids with $v = 2/3$ [28] and parafermion particle zero modes [29].

In the metaplectic anyons system $SO(p)_2$, the simple objects (anyon types) are denoted as $\{1, X_\epsilon, Y_j, X'_\epsilon, Z, 1 \leq j \leq r\}$, where $p = 2r + 1$. The case of $p=3$ is the center of our interest, in this

* jxzhong@xtu.edu.cn

† ljmeng@xtu.edu.cn

case $SO(3)_2 = SU(2)_4$, the simple objects become $\{1, X_\epsilon, Y, X'_\epsilon, Z\}$ and their corresponding topological spins are $\{0, 1/2, 1, 3/2, 2\}$, following reference [26], which labeled them twice topological spins $\{0, 1, 2, 3, 4\}$. For simplicity, we use X/X' for X_ϵ/X'_ϵ later.

According to the k-level theory of fusion rules [30], the topological spins s_1 and s_2 can be fusion (recoupling, \otimes) and give total coupling spins

$$s_1 \otimes s_2 = |s_1 - s_2| \oplus |s_1 - s_2| + 1 \dots \dots \oplus \min(s_1 + s_2, k - s_1 - s_2), \quad (1)$$

where \otimes and \oplus denote direct product and direct sum respectively. In Eq .(1) combined with the topological spins of the metaplectic anyons, we can get all the fusion rules that need to be used:

$$\begin{aligned} X \otimes X &= 1 \oplus Y, X \otimes Y = X \oplus X', X \otimes X' = Y \oplus Z, \\ X' \otimes Z &= X', Y \otimes Y = 1 \oplus Y \oplus Z, Y \otimes X' = X \oplus X', \\ Y \otimes Z &= Y, X' \otimes X' = 1 \oplus Y, X' \otimes Z = X, Z \otimes Z = 1. \end{aligned} \quad (2)$$

Note that we do not present the fusion rules of anyons and vacuum. Based on the above fusion rules, combining several F -matrices and R -symbols of metaplectic anyons, we can obtain EBMs for constructing standard quantum gates, including one-qubit and two-qubit gates. The standard set of universal gates for qubit quantum circuit models consists of a Hadamard gate H , a phase gate T , and a controlled-not gate CNOT [31, 32]. Therefore, it is important to construct the set of those quantum gates using EBMs and measure the distance of a braidword from a standard qubit gate as the precision index of the constructed quantum gate.

Cui and Wang demonstrated [26] that the combination of the braidings of the anyon X and the projective measurement of the total charge of the two metaplectic anyons can implement universal quantum computing. Previous studies identified the universality of a qutrit model V_2^{1111} and a qubit model V_0^{1111} [26], V_0^{2222} and V_0^{1221} models [33]. For constructing a two-qubit gate, we can choose to use 8 anyons (4 anyons corresponding to one qubit) [21, 26, 34] or 6 anyons (3 anyons corresponding to one qubit) [17, 35, 36]. We choose the latter (6 anyons) to construct a two-qubit gate because the number of redundant non-computational states can be reduced effectively. As a consequence, the dimension of EBMs can be kept at a low-rank level, which is conducive to the solution of EBMs of a two-qubit gate. Standard encoding uses three or four X with a topological spin of 1/2, and universal quantum computing cannot be implemented under this limitation in $SO(3)_2$. But it has been shown that braiding with fusion and measurement together can achieve a universal set of gates [37]. By introducing a pair of Z anyons after braiding X and X' once, the arrangement of initial state anyons can be recovered without affecting the intermediate state, which makes non-standard coding feasible. In this process, fusion is necessary, but measurement does not seem to be

necessary. There are 6 qubit models in the metaplectic anyon model with 3 anyons encoding, among which 3 models $\{V_3^{113}, V_3^{131}, V_1^{133}\}$ are selected for the systematic construction of one/two-qubit gate, refer to Appendix A for a detailed analysis procedure.

The structure of this article is as follows. In the part II, we give the one-qubit EBMs of $\{V_3^{113}, V_3^{131}, V_1^{133}\}$, and show the results of constructing H - and T -gates which are optimized by GA-enhanced SKA. In the part III, we present the EBMs of $\{V_3^{113}, V_3^{131}, V_1^{133}\}$ for constructing two-qubit gates, and show the approximation of braidword to a local equivalence class of CNOT-gates. In the part IV, we summarize our results. Appendix A analyzes the process of selecting the optimal qubit model among all metaplectic anyon models with 3 anyons encoding. Appendix B lists all the basis transformation matrices F and exchange phases R used to derive all EBMs. Appendix C gives the specific braiding calculation processes for obtaining the $\sigma_2^{(3)}/\sigma_3^{(6)}$ EBMs.

II. THE CONSTRUCTION OF ONE-QUBIT GATE

In topological quantum computing, intermediate fusion states are used to represent qubits. Three anyons can build a one-qubit. Fig. 1 shows the fusion processes of $\{V_3^{113}, V_3^{131}, V_1^{133}\}$ models for constructing one-qubit gates. Specifically, in the initial state, we arrange three anyons (X, X, X') for V_3^{113} , (X, X', X) for V_3^{131} and (X, X', X') for V_1^{133} , X_i would be equal to either $1/Y$ (Fig. 1(a)) or Y/Z (Fig. 1(b) and Fig. 1(c)) according to the fusion rules Eq .(2). Consequently, for V_3^{113} , we can obtain binary states through endowing with $X_i = 1$ and Y encoding $|0\rangle$ and $|1\rangle$, respectively, and then they are finally fusion into X' . These two fusion processes are simply denoted as $|0\rangle = ((X, X)_1, X')_{X'}$, $|1\rangle = ((X, X)_Y, X')_{X'}$. Similarly, the binary states are $|0\rangle = ((X, X')_Y, X)_{X'}$, $|1\rangle = ((X, X')_Z, X)_{X'}$ for V_3^{131} and $|0\rangle = ((X, X')_Y, X')_X$, $|1\rangle = ((X, X')_Z, X')_X$ for V_1^{133} .

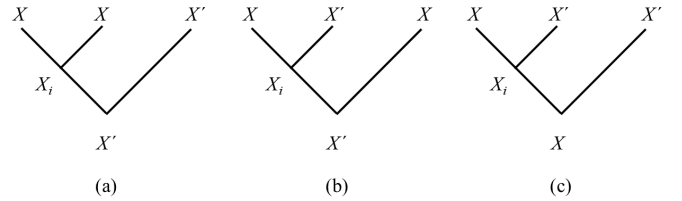


FIG. 1: (a) The model V_3^{113} . The initial state is composed of two anyons X and one X' anyon, which are finally fused into one X' anyon. (b) The model V_3^{131} . Three initial metaplectic anyons X, X', X are fused into one anyon X' . (c) The model V_1^{133} . Three initial metaplectic anyons X, X', X' are fused into one anyon X .

Although both V_3^{113} and V_3^{131} are initially made up of two X and one X' , and fusing into X' eventually,

the different order of fusion results in different intermediate states. In contrast, and have the same intermediate state, but the initial and final fused anyons are different. These two differences can lead to different EBMs. The EBMs $\sigma_i^{(3)} (i = 1, 2)$ corresponds to the braiding of the i anyon with the $i+1$ anyon, noting that the superscript (3) represents the 3 anyons of the one-qubit, similarly the 6 anyons in the two-qubit EBMs $\sigma_i^{(6)}$. It is easy for $\sigma_1^{(3)}$ to solve, because we only need to braid the first and

second anyons (starting from the most left one), and only need to use the R -symbols. However, it is slightly complicated to solve $\sigma_2^{(3)}$, which involves braiding the second and third anyons, due to basis transformation which is necessary to use F -matrices and R -symbols simultaneously. The specific solving processes are given in Appendix C. All F -matrices and R -symbols used in solving EBMs are summarized in Appendix B.

For the $\{V_3^{113}, V_3^{131}, V_1^{133}\}$ models, we get the EBMs as follows:

$$\begin{aligned} V_3^{113} : \sigma_1^{(3)} &= \begin{bmatrix} e^{i\frac{3\pi}{4}} & 0 \\ 0 & e^{i\frac{\pi}{12}} \end{bmatrix}, \sigma_2^{(3)} = \frac{1}{3} \begin{bmatrix} 2e^{i\frac{7\pi}{12}} + e^{i\frac{\pi}{4}} & -\sqrt{2}e^{i\frac{7\pi}{12}} + \sqrt{2}e^{i\frac{\pi}{4}} \\ -\sqrt{2}e^{i\frac{7\pi}{12}} + \sqrt{2}e^{i\frac{\pi}{4}} & e^{i\frac{7\pi}{12}} + 2e^{i\frac{\pi}{4}} \end{bmatrix}; \\ V_3^{131} : \sigma_1^{(3)} &= \begin{bmatrix} e^{i\frac{7\pi}{12}} & 0 \\ 0 & e^{i\frac{\pi}{4}} \end{bmatrix}, \sigma_2^{(3)} = \frac{1}{3} \begin{bmatrix} e^{i\frac{7\pi}{12}} + 2e^{i\frac{\pi}{4}} & -\sqrt{2}e^{i\frac{7\pi}{12}} + \sqrt{2}e^{i\frac{\pi}{4}} \\ -\sqrt{2}e^{i\frac{7\pi}{12}} + \sqrt{2}e^{i\frac{\pi}{4}} & 2e^{i\frac{7\pi}{12}} + e^{i\frac{\pi}{4}} \end{bmatrix}; \\ V_1^{133} : \sigma_1^{(3)} &= \begin{bmatrix} e^{i\frac{7\pi}{12}} & 0 \\ 0 & e^{i\frac{\pi}{4}} \end{bmatrix}, \sigma_2^{(3)} = \frac{1}{3} \begin{bmatrix} 2e^{-i\frac{\pi}{4}} + e^{-i\frac{11\pi}{12}} & -\sqrt{2}e^{-i\frac{\pi}{4}} + \sqrt{2}e^{-i\frac{11\pi}{12}} \\ -\sqrt{2}e^{-i\frac{\pi}{4}} + \sqrt{2}e^{-i\frac{11\pi}{12}} & e^{-i\frac{\pi}{4}} + 2e^{-i\frac{11\pi}{12}} \end{bmatrix}. \end{aligned}$$

Standard H/T -gate cannot be constructed directly using EBMs of $\{V_3^{113}, V_3^{131}, V_1^{133}\}$ models, similar to the Fibonacci anyon model, only a braidword from the braiding of EBMs approximation to H/T -gate can be obtained, which becomes a quantum compilation problem. To measure the distance between a braidword and a standard gate, we use the global phase invariant distance [34]:

$$d(U_0, U) = \sqrt{1 - \frac{|\text{tr}(U_0 U^\dagger)|}{2}} \quad (3)$$

where U_0 represents a matrix of the standard one-qubit gate and U represents the matrix of braidword obtained by the arrangement of EBMs, and Tr denotes the trace of the matrix $U_0 U^\dagger$. A smaller distance $d(U_0, U)$ indicates a smaller error between the braidword and the standard gate.

For the one-qubit compilation problem, our solution is the GA-enhanced SKA [38]. The SKA promises an exponentially reduced distance at the cost of each five-times increase in length (the number of EBMs) by recursive calls [13]. The limitation of the traditional SKA is that 0-order approximations need to be obtained using exhaustive search, which quickly becomes infeasible for basic lengths greater than 14. E. G. Johansen replaced exhaustive search with the Monte Carlo method in the 0-order approximation [14], which resulted in significant performance improvements, including unlimited basic length and a great reduction in time cost. Inspired by Monte Carlo-enhanced SKA, we use GA to replace exhaustive search in 0-level approximation, which has similar advantages. Specific practices are as follows:

i A braidword / many braidwords / global phase invariant distance corresponds to an individual / a group / fitness.

ii To randomly generate a number of braidwords, to produce a new generation of groups through hybridization and mutation as the parent's text.

iii Retaining some individuals with high fitness (low global phase invariant distance) in the parent's text.

iv A new generation of population is generated by hybridization and mutation of the parent's text while retaining a part of the population with high fitness as the new parent's text.

v Repeat steps iii and iv until reach the hybridization generation we set.

vi The individual with the highest final output fitness is used as the 0-order approximation required by SKA.

Each 0-level approximation is found by GA. We run the GA three times and select the individual with the highest fitness for calculations. By recursively calling SKA, we can further obtain the 1-, 2-, and 3-level approximations for H - and T -gates.

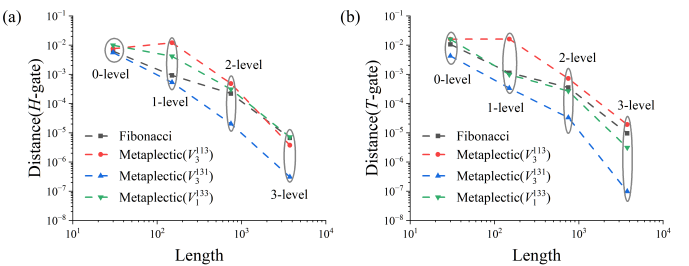


FIG. 2: The $\{V_3^{113}, V_3^{131}, V_1^{133}\}$ model uses GA-enhanced SKA to obtain 0-, 1-, 2-, and 3-level approximations of the (a) H-gate and (b) T-gate. The basic length $L_0=30$ is set.

Setting the same parameters in GA, we obtain the results shown in Fig. 2 by running the GA-enhanced SKA algorithm on $\{\text{Fibonacci}, V_3^{113}, V_3^{131}, V_1^{133}\}$ four models, respectively. For the approximation of the standard H -gate, Fig. 2(a) shows that the V_3^{131} model performs best at all levels of approximation, and V_3^{113}/V_1^{133} can achieve a comparable distance (10^{-5}) with the Fibonacci model at the 3-level approximation. The threshold theorem re-

quires that the error between the braidword and the standard qubit gate is less than 1% [39–44], which means that our $d(U_0, U)$ from the standard gate needs to be less than (10^{-2}) . For the V_3^{131} model, we only need to achieve the 1-level approximation (corresponding to 30×5^1 braid operations) to meet the computational requirements. For the $\{\text{Fibonacci}, V_3^{113}, V_1^{133}\}$ model, we need to achieve a 2-level approximation (corresponding to 30×5^2 braid operations), so choosing V_3^{131} for calculations can reduce a number of unnecessary braid operations. Fig. 2(b) demonstrates the best performance when approximating the standard T -gate for the model V_3^{131} . Similar to the H -gate approximation, to meet the requirements of the threshold theorem, we need to achieve a 1-order approximation for V_3^{131} and a 2-order approximation for $\{\text{Fibonacci}, V_3^{113}, V_1^{133}\}$.

III. THE CONSTRUCTION OF TWO-QUBIT GATES

Encoding two-qubit requires the use of 6 anyons for our model. Fig. 3(a) shows the computational and non-computational states of the two-qubit model for V_3^{113} . We first arrange four anyons X and two anyons X' , then finally fuse them into the vacuum. According to the fusion rules, four computational states $|X_i X_j\rangle (|11\rangle, |1Y\rangle, |Y1\rangle, |YY\rangle)$ will be generated in the fusion processes, and we can encode them corresponding as $(|00\rangle, |01\rangle, |10\rangle, |11\rangle)$, a non-computational state

$|NC\rangle$ will produce simultaneously, similar to the Fibonacci model with 6 anyons code. Similarly, Fig. 3(b) shows the computational state $(|YY\rangle, |YZ\rangle, |ZY\rangle, |ZZ\rangle)$, which also correspond to $(|00\rangle, |01\rangle, |10\rangle, |11\rangle)$ and non-computational state for V_3^{131} , and Fig. 3(c) shows the computational state $(|YY\rangle, |YZ\rangle, |ZY\rangle)$ and non-computational states for V_1^{133} . Note that V_3^{131} and V_1^{133} have the same encoding intermediate state, but differences in the initial anyons result in different EBMs.

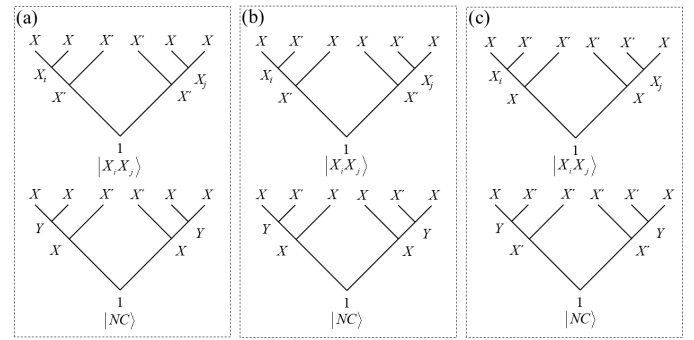


FIG. 3: The top/bottom figures correspond to the computational/non-computational states. (a) The two-qubit model of V_3^{113} ; (b) The two-qubit model of V_3^{131} ; (c) The two-qubit model of V_1^{133} .

For encoding two-qubit, in the case of basic vectors $(|NC\rangle, |11\rangle, |1Y\rangle, |Y1\rangle, |YY\rangle)$ for V_3^{113} , $(|NC\rangle, |YY\rangle, |YZ\rangle, |ZY\rangle, |ZZ\rangle)$ for $V_3^{131}(V_1^{133})$, we obtain the EBMs as follows:

V_3^{113} :

$$\sigma_1^{(6)} = R_2^{11} \oplus (\sigma_1^{(3)} \otimes I_2), \sigma_2^{(6)} = R_2^{13} \oplus (\sigma_2^{(3)} \otimes I_2),$$

$$\sigma_3^{(6)} = \frac{1}{2} \begin{bmatrix} e^{-i\frac{\pi}{4}} + e^{-i\frac{11\pi}{12}} & 0 & 0 & 0 & -e^{-i\frac{\pi}{4}} + e^{-i\frac{11\pi}{12}} \\ 0 & 2e^{-i\frac{\pi}{4}} & 0 & 0 & 0 \\ 0 & 0 & 2e^{-i\frac{11\pi}{12}} & 0 & 0 \\ 0 & 0 & 0 & 2e^{-i\frac{11\pi}{12}} & 0 \\ -e^{-i\frac{\pi}{4}} + e^{-i\frac{11\pi}{12}} & 0 & 0 & 0 & e^{-i\frac{\pi}{4}} + e^{-i\frac{11\pi}{12}} \end{bmatrix},$$

$$\sigma_4^{(6)} = R_2^{31} \oplus (I_2 \otimes \sigma_1^{(3)}), \sigma_5^{(6)} = R_2^{11} \oplus (I_2 \otimes \sigma_2^{(3)}).$$

V_3^{131} :

$$\sigma_1^{(6)} = R_2^{13} \oplus (\sigma_1^{(3)} \otimes I_2), \sigma_2^{(6)} = R_2^{31} \oplus (\sigma_2^{(3)} \otimes I_2),$$

$$\sigma_3^{(6)} = \frac{1}{2} \begin{bmatrix} e^{i\frac{3\pi}{4}} + e^{i\frac{\pi}{12}} & -e^{i\frac{3\pi}{4}} + e^{i\frac{\pi}{12}} & 0 & 0 & 0 \\ -e^{i\frac{3\pi}{4}} + e^{i\frac{\pi}{12}} & e^{i\frac{3\pi}{4}} + e^{i\frac{\pi}{12}} & 0 & 0 & 0 \\ 0 & 0 & 2e^{-i\frac{\pi}{12}} & 0 & 0 \\ 0 & 0 & 0 & 2e^{-i\frac{\pi}{12}} & 0 \\ 0 & 0 & 0 & 0 & 2e^{i\frac{3\pi}{4}} \end{bmatrix},$$

$$\sigma_4^{(6)} = R_2^{13} \oplus (I_2 \otimes \sigma_1^{(3)}), \sigma_5^{(6)} = R_2^{31} \oplus (I_2 \otimes \sigma_2^{(3)}).$$

V_1^{133} :

$$\sigma_1^{(6)} = R_2^{13} \oplus (\sigma_1^{(3)} \otimes I_2), \sigma_2^{(6)} = R_2^{33} \oplus (\sigma_2^{(3)} \otimes I_2),$$

$$\sigma_3^{(6)} = \frac{1}{2} \begin{bmatrix} e^{-i\frac{\pi}{4}} + e^{-i\frac{11\pi}{12}} & -e^{-i\frac{\pi}{4}} + e^{-i\frac{11\pi}{12}} & 0 & 0 & 0 \\ -e^{-i\frac{\pi}{4}} + e^{-i\frac{11\pi}{12}} & e^{-i\frac{\pi}{4}} + e^{-i\frac{11\pi}{12}} & 0 & 0 & 0 \\ 0 & 0 & 2e^{-i\frac{11\pi}{12}} & 0 & 0 \\ 0 & 0 & 0 & 2e^{-i\frac{11\pi}{12}} & 0 \\ 0 & 0 & 0 & 0 & 2e^{-i\frac{\pi}{4}} \end{bmatrix},$$

$$\sigma_4^{(6)} = R_2^{33} \oplus (I_2 \otimes \sigma_1^{(3)}), \sigma_5^{(6)} = R_2^{31} \oplus (I_2 \otimes \sigma_2^{(3)}).$$

For the $\sigma_1^{(6)}/\sigma_5^{(6)}$ is easy to get, we only need to braid the first/last two anyons, only R -symbols need to be used. The solution of the $\sigma_2^{(6)}/\sigma_3^{(6)}/\sigma_4^{(6)}$ is much more complicated, and it needs to change the basis to a braid corresponding to two anyons, F -matrices and R -symbols should be used simultaneously, and the specific solution process for $\sigma_3^{(6)}$ is referred to Appendix C.

For the $V_3^{113}, V_3^{131}, V_1^{133}$ models, there is a direct product relationship between the EBMs $\sigma_1^{(6)}/\sigma_2^{(6)}/\sigma_4^{(6)}/\sigma_5^{(6)}$ of the two-qubit gates and the EBMs $\sigma_1^{(3)}/\sigma_2^{(3)}$ of the one-qubit, but there is no such relationship for $\sigma_3^{(6)}$, which indicates the entanglement of two qubits.

Among the two-qubit gates, CNOT-gate is the key, and it can be combined with H -gate and T -gate to realize universal quantum computing. The braidword formed using the five EBMs of $\{V_3^{113}, V_3^{131}, V_1^{133}\}$ is a 5-dimensional matrix, and we write the braidword as $B = M_{11} \oplus A$ so that M_{11} corresponds to the non-computational space and $|M_{11}| = \sqrt{M_{11}M_{11}^\dagger} \approx 1$ [19], A corresponds to the 4-dimensional computational space matrix. To construct the CNOT-gate, we try to approximate a local equivalence class of the CNOT-gate with the A -matrix [45]. Following the work [20], we convert the U (which can be a standard two-qubit gate or a computational matrix A in a braidword) from a standard computational basis to a Bell basis,

$$U_B = Q^\dagger U Q, Q = \frac{1}{\sqrt{2}} \begin{bmatrix} 1 & 0 & 0 & i \\ 0 & i & 1 & 0 \\ 0 & i & -1 & 0 \\ 1 & 0 & 0 & -i \end{bmatrix} \quad (4)$$

then obtain three real parameters g_1, g_2, g_3 called local invariants:

$$g_1 = \text{Re}\left\{\frac{\text{tr}^2(m_u)}{16 \cdot U}\right\},$$

$$g_2 = \text{Im}\left\{\frac{\text{tr}^2(m_u)}{16 \cdot U}\right\}, \quad (5)$$

$$g_3 = \frac{\text{tr}^2(m_u) - \text{tr}(m_u^2)}{4 \cdot U}$$

where $m_u = U_B^T U_B$. These formulas provided in the reference [20] are used to measure the distance between the braidword and the local invariant of the CNOT-gate,

$$d^{CNOT}(A) = \sum_{i=1}^3 \Delta g_i^2, \Delta g_i = |g_i(A) - g_i(\text{CNOT})| \quad (6)$$

where A is the computational matrix in the braidword, and the g_1, g_2, g_3 of CNOT-gate can be obtained directly by Eq.(4) and Eq.(5), they are

$$g_1(\text{CNOT}) = 0, g_2(\text{CNOT}) = 0, g_3(\text{CNOT}) = 1$$

At the same time, to ensure that the A -matrix is approximately unitary, we also make unitary measurements of A :

$$d^U = \text{Tr}(\sqrt{a^\dagger a}), \quad a = A^\dagger A - I \quad (7)$$

where I is a 4-dimensional identity matrix.

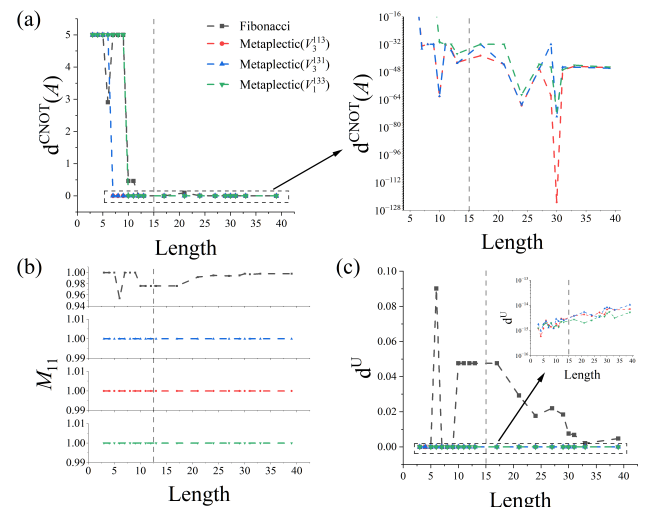


FIG. 4: The distance of local equivalence class [CNOT] and unitary measurement without inverse EBMs. (a) The distance between the {Fibonacci, $V_3^{113}, V_3^{131}, V_1^{133}$ } models and the local equivalence class [CNOT] at different lengths. We use exhaustive search at short lengths, and GA at long lengths. The gray dashed line distinguishes the two methods. (b) M_{11} for {Fibonacci, $V_3^{113}, V_3^{131}, V_1^{133}$ }. (c) Unitary measurement of A -matrix for {Fibonacci, $V_3^{113}, V_3^{131}, V_1^{133}$ }.

Note the data of the Fibonacci model in Fig. 4 and Fig. 5 comes from [20]. For exhaustive search based on 5/10 kinds of EBMs, the length reaches 13/7. The inverse matrix is not added to our calculations so that the exhaustive search can reach a longer length. The GA is used for the length larger than the upper limit of the exhaustive search, and the results are shown in Fig. 4. The results show that the V_3^{113} approximation of a local equivalence class for CNOT-gate is satisfactory, even reaches close to 10^{-128} when the length is

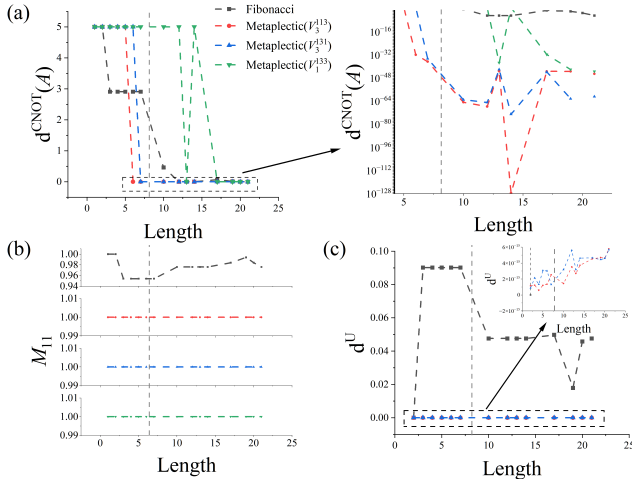


FIG. 5: The distance of local equivalence class [CNOT] and unitary measurement with inverse EBMs. (a) The distance between the $\{\text{Fibonacci}, V_3^{113}, V_3^{131}, V_1^{133}\}$ models and the local equivalence class [CNOT] at different lengths. We use exhaustive search at short lengths, and GA at long lengths. The gray dashed line distinguishes the two methods. (b) M_{11} for $\{\text{Fibonacci}, V_3^{113}, V_3^{131}, V_1^{133}\}$. (c) Unitary measurement of A -matrix for $\{\text{Fibonacci}, V_3^{113}, V_3^{131}, V_1^{133}\}$.

30, which is far less than the other three models (Fig. 4(a)). The distance of the local equivalence class decreases rapidly (reaching below 10^{-32}) when the length is greater than 10 for $\{V_3^{113}, V_3^{131}, V_1^{133}\}$, far less than the Fibonacci model. The value of M_{11} can remain in a straight line for $\{V_3^{113}, V_3^{131}, V_1^{133}\}$, but the Fibonacci model produces some considerable fluctuations. The unitary measurement of $\{V_3^{113}, V_3^{131}, V_1^{133}\}$ for the A -matrix can always be kept at an ideal value (below 10^{-14}), which is generally better than the Fibonacci model. The calculation results of adding the inverse matrices are shown in Fig. 5. The conclusion is consistent with no inverse matrices, V_3^{113} giving the best result in all models. Compared with the case without the inverse matrices, V_3^{113} only needs $l = 14$ to reach 10^{-128} approximately. At the same time, we find that when the inverse matrices are added, three models find a braidword with a distance equal to 0 (below 10^{-128}) from the local equivalence class [CNOT] when the length is 20. We show these three braidwords in Table I. The M_{11} of $\{V_3^{113}, V_3^{131}, V_1^{133}\}$ always remains equal to 1, which M_{11} of the Fibonacci model is often far from 1 for comparison. For unitary measurements of the A -matrix, the results indicate that three models $\{V_3^{113}, V_3^{131}, V_1^{133}\}$ can reach an excellent level (below 6×10^{-15}), superior to the Fibonacci model.

TABLE I: The braidwords of three models with the local equivalent class [CNOT] distance equal 0 at length 20, and corresponding M_{11} and unitary measurements of A -matrix. The A/B/C/D/E/F/G/H/I/J represents $\sigma_1^{(6)}/\sigma_2^{(6)}/\sigma_3^{(6)}/\sigma_4^{(6)}/\sigma_5^{(6)}/\sigma_1^{(6)-1}/\sigma_2^{(6)-1}/\sigma_3^{(6)-1}/\sigma_4^{(6)-1}/\sigma_5^{(6)-1}$, respectively.

Model	braidword	distance	M_{11}	Unitary measurement(A)
V_3^{113}	BBIFBDAAHFJBAHBHBBJA	0	1	4.629×10^{-15}
V_3^{131}	GFEAGJCBAAHHBCBBBJB	0	1	4.586×10^{-15}
V_1^{133}	DGIGJHBFBEFFCBFBHBF	0	1	2.554×10^{-15}

IV. CONCLUSIONS

We investigate the metaplectic anyon models based on $SO(3)_2$ and obtain 6 anyon models according to F -matrices/ R -symbols and fusion rules by non-standard encoding. By adding a pair of Z anyons after braiding X with X' , the initial arrangement of anyons can be reset, which makes it feasible to obtain the corresponding EBMs. We emphasize that only auxiliary anyons are added for fusion in this process, which means that measurements may not be necessary to implement a universal set of gates for $SO(3)_2$ anyon model. The models of EBMs with global phase differences are grouped into one class, we select the best three models $\{V_3^{113}, V_3^{131}, V_1^{133}\}$ for systematic study. Utilizing F -matrices and R -symbols, we solve analytically the corresponding one-/two-qubit EBMs of these three models. For the one-qubit case, we use the global phase invariant distance as a metric, and based on the one-qubit EBMs, we use GA-enhanced SKA to construct a standard H/T -gate, then compare it

with the Fibonacci model. The calculation results show that V_3^{131} gives the best performance, although V_3^{113} and V_1^{133} are slightly inferior to the Fibonacci model at 0- and 1-level approximations, they are comparable to the Fibonacci model at 2- or 3-level approximations. For the two-qubit case, we try to approximate a local equivalence class of the CNOT-gate. Based on the two-qubit EBMs, we use exhaustive search/GA to get the ideal braidword when the length is short/long. Compared with the Fibonacci model, the calculation results show that our model has obvious advantages, $\{V_3^{113}, V_3^{131}, V_1^{133}\}$ can obtain far higher precision (below 10^{-32}). All three models with inverse EBMs find a braidword with $l = 20$ and local equivalence class with distance equals 0. At the same time, the unitary measurement of the computational matrix always is better than the well-known Fibonacci model. Our work increases the number of topological quantum computing models based on metaplectic anyons and is expected to be applied to future topological quantum computing.

Acknowledgments This work is supported by the National Natural Science Foundation of China (Grant Nos. 12374046, 11204261), College of Physics and Optoelectronic Engineering training program, a Key Project of the Education Department of Hunan Province (Grant No. 19A471), Natural Science Foundation of Hunan Province (Grant No. 2018JJ2381).

Appendix A: The process of selecting available models

According to the fusion rules, qubits can be constructed requiring that the fusion result of the intermediate state have two kinds of anyons corresponding to the $|0\rangle$ and $|1\rangle$. The following fusion rules must be applied:

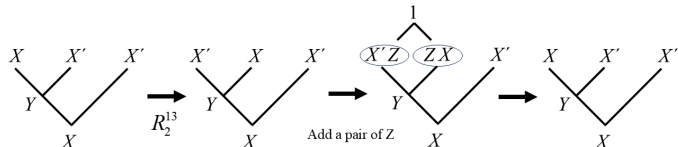
$$X \otimes X = 1 \oplus Y, X \otimes Y = X \oplus X', X \otimes X' = Y \oplus Z, \quad (A1)$$

$$Y \otimes X' = X \oplus X', X' \otimes X' = 1 \oplus Y.$$

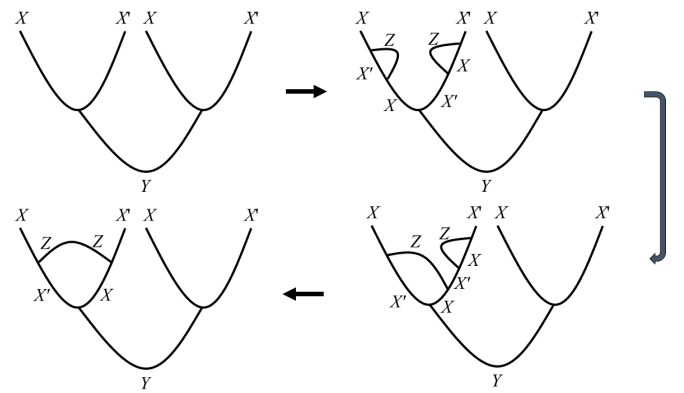
Three anyons construct qubit, the first and second anyons correspond to the two anyons of the above fusion rule, and the third anyon is selected from $\{1, X, Y, X', Z\}$ to obtain the following model:

$$V_1^{111}, V_2^{112}, V_3^{113}, V_1^{331}, V_2^{332}, V_3^{333}, V_2^{121}, \\ V_1^{122}, V_2^{122}, V_3^{123}, V_2^{211}, V_1^{212}, V_3^{212}, V_2^{213}, \\ V_3^{131}, V_2^{132}, V_1^{133}, V_3^{311}, V_2^{312}, V_1^{313}, V_2^{231}, \\ V_1^{232}, V_3^{232}, V_2^{233}, V_2^{321}, V_1^{322}, V_3^{322}, V_2^{323}.$$

There are 28 possible models in total. With the exception of the standard encodings V_1^{111} and V_3^{333} , non-standard encodings are unusable due to state changes (changes in anyons initial order) after a single exchange. In the model of adjacent different kinds of anyons, we make the model with only 1 and 3 adjacent can be used by introducing a pair of Z anyons after braiding for once:



The fusion rule with Z is Abelian, the fusion of the other anyons with Z produces the only one anyon. we notice that $X \otimes Z = X'$ and $X' \otimes Z = X$, means X switches with X' , which is exactly what we want. But this is not true for X adjacent to Y or X' adjacent to Y . The only thing we have to worry about is whether the introduction of a pair of Z -anyons will have any effect on the fusion result, fortunately it won't, and we can understand this through the following process:



Y doesn't convert to Z in this process.
Only the following models can be used:

$$V_1^{111}, V_3^{333}, V_3^{113}, V_1^{331}, V_3^{131}, V_1^{133}, V_3^{311}, V_1^{311}, V_3^{313}$$

If we brading X and X' , we can return to the original state by introducing a pair of Z anyons, and braiding the same kind of anyons requires no additional processing. The $\sigma_1^{(3)}$ and $\sigma_2^{(3)}$ of all the above models are solved and the corresponding EMBs $\{\sigma_1^{(6)}, \sigma_2^{(6)}, \sigma_4^{(6)}, \sigma_5^{(6)}\}$ of local equivalent class of two-qubit gates can also be obtained easily by direct sum and direct product. Such as:

$$\sigma_1^{(6)} = R \oplus (\sigma_1^{(3)} \otimes I_2), \sigma_2^{(6)} = R \oplus (\sigma_2^{(3)} \otimes I_2), \\ \sigma_4^{(6)} = R \oplus (I_2 \otimes \sigma_1^{(3)}), \sigma_5^{(6)} = R \oplus (I_2 \otimes \sigma_2^{(3)}).$$

Only $\sigma_3^{(6)}$ must be obtained by processing of braiding the third and fourth anyons. Then we can construct one-qubit H -/ T -gates and two-qubit local equivalent class [CNOT] using these EMBs, and we find V_1^{111} and V_3^{333} construct H -/ T -gates failure.

We put together the remaining 6 models in Table II which the one-qubit EMBs differ only by a global phase:

TABLE II: The 6 models of three anyons based on $SO(3)_2$.

Model	Phase difference
V_3^{113}/V_1^{331}	$\sigma_1^{(3)}(\pi)$
V_3^{131}/V_1^{313}	same
V_3^{311}/V_1^{133}	$\sigma_2^{(3)}(\pi)$

The phase difference between the first model and the second model in the summarized in parentheses.

For one-qubit, the same braidword formed by a set of EMBs that differ by a global phase has the same result calculated using the global phase invariant distance formula. However, for two-qubit, the same braidword is constructed by two sets of EMBs with a global phase difference, and the distance from CNOT-gate is calculated using local equivalence class, and different results are obtained.

We use an exhaustive search to find the minimum value of local equivalence class [CNOT] distance at each length for these six models. The result are presented in Table III and Table IV.

TABLE III: The minimum distances of local equivalence class [CNOT]. The inverse matrices are not added.

Length	V_3^{113}	V_1^{331}	V_3^{131}	V_1^{313}	V_3^{311}	V_1^{133}
3	5	5	5	5	5	5
4	5	5	5	5	5	5
5	5	5	5	5	5	5
6	5	5	5	5	5	5
7	1.28×10^{-33}	5	2.70×10^{-35}	1.83×10^{-32}	5	5
8	1.23×10^{-32}	5	1.23×10^{-32}	1.23×10^{-32}	5	5
9	1.23×10^{-32}	5	1.23×10^{-32}	1.23×10^{-32}	5	5
10	9.46×10^{-63}	1.79	1.16×10^{-62}	2.57×10^{-62}	2.48×10^{-32}	1.98×10^{-31}
11	1.23×10^{-32}	3.11×10^{-3}	1.23×10^{-32}	1.23×10^{-32}	1.23×10^{-32}	1.23×10^{-32}
12	3.26×10^{-35}	9.80×10^{-6}	3.08×10^{-36}	3.24×10^{-34}	1.23×10^{-32}	1.23×10^{-32}
13	3.75×10^{-43}	2.36×10^{-8}	1.24×10^{-43}	2.38×10^{-43}	7.24×10^{-37}	4.00×10^{-38}

TABLE IV: The minimum distances of local equivalence class [CNOT]. The inverse matrices are added.

Length	V_3^{113}	V_1^{331}	V_3^{131}	V_1^{313}	V_3^{311}	V_1^{133}
3	5	5	5	5	5	5
4	5	5	5	5	5	5
5	5	5	5	5	5	5
6	1.23×10^{-32}	5	5	5.00×10^{-5}	5	5
7	2.37×10^{-37}	4.40	2.70×10^{-35}	1.23×10^{-32}	5	5

We can find that V_3^{113} was significantly better than V_1^{331} , and the other two groups were not much different. We choose $\{V_3^{113}, V_3^{131}, V_1^{133}\}$ for the study of constructing a standard quantum gate systematically.

Appendix B: The all of F -matrices and R -symbols used to solve BEMs

We list the F -matrices and R -symbols for $\{V_3^{113}, V_3^{131}, V_1^{133}\}$ as follows:

For model V_3^{113} :

$$F_3^{113} = \begin{bmatrix} F_{3;20}^{113} & F_{3;40}^{113} \\ F_{3;40}^{113} & F_{3;42}^{113} \end{bmatrix} = \frac{1}{\sqrt{3}} \begin{bmatrix} -\sqrt{2} & 1 \\ 1 & \sqrt{2} \end{bmatrix},$$

$$F_3^{311} = \begin{bmatrix} F_{3;02}^{311} & F_{3;04}^{311} \\ F_{3;22}^{311} & F_{3;24}^{311} \end{bmatrix} = \frac{1}{\sqrt{3}} \begin{bmatrix} -\sqrt{2} & 1 \\ 1 & \sqrt{2} \end{bmatrix},$$

$$F_2^{332} = \begin{bmatrix} F_{2;10}^{332} & F_{2;12}^{332} \\ F_{2;30}^{332} & F_{2;32}^{332} \end{bmatrix} = \frac{1}{\sqrt{2}} \begin{bmatrix} 1 & -1 \\ -1 & 1 \end{bmatrix},$$

$$R_0^{11} = e^{i\frac{3\pi}{4}}, R_2^{11} = e^{i\frac{\pi}{12}}, R_2^{13} = R_2^{31} = e^{i\frac{7\pi}{12}}, R_4^{13} = R_4^{31} = e^{i\frac{\pi}{4}}, R_4^{33} = e^{-i\frac{\pi}{4}}, R_2^{33} = e^{-i\frac{11\pi}{12}}.$$

For model V_3^{131} :

$$F_2^{112} = \begin{bmatrix} F_{2;10}^{112} & F_{2;12}^{112} \\ F_{2;30}^{112} & F_{2;32}^{112} \end{bmatrix} = \frac{1}{\sqrt{2}} \begin{bmatrix} -1 & 1 \\ 1 & 1 \end{bmatrix},$$

$$F_3^{131} = \begin{bmatrix} F_{3;22}^{131} & F_{3;24}^{131} \\ F_{3;42}^{131} & F_{3;44}^{131} \end{bmatrix} = \frac{1}{\sqrt{3}} \begin{bmatrix} -1 & \sqrt{2} \\ \sqrt{2} & 1 \end{bmatrix},$$

$$R_0^{11} = e^{i\frac{3\pi}{4}}, R_2^{11} = e^{i\frac{\pi}{12}}, R_2^{13} = R_2^{31} = e^{i\frac{7\pi}{12}}, R_4^{13} = R_4^{31} = e^{i\frac{\pi}{4}}, R_4^{33} = e^{-i\frac{\pi}{4}}, R_2^{33} = e^{-i\frac{11\pi}{12}}.$$

For model V_1^{133} :

$$F_1^{133} = \begin{bmatrix} F_{1;02}^{133} & F_{1;04}^{133} \\ F_{1;22}^{133} & F_{1;24}^{133} \end{bmatrix} = \frac{1}{\sqrt{3}} \begin{bmatrix} -\sqrt{2} & 1 \\ 1 & \sqrt{2} \end{bmatrix},$$

$$F_1^{331} = \begin{bmatrix} F_{1;20}^{331} & F_{1;22}^{331} \\ F_{1;40}^{331} & F_{1;42}^{331} \end{bmatrix} = \frac{1}{\sqrt{3}} \begin{bmatrix} -\sqrt{2} & 1 \\ 1 & \sqrt{2} \end{bmatrix},$$

$$F_2^{332} = \begin{bmatrix} F_{2;10}^{332} & F_{2;12}^{332} \\ F_{2;30}^{332} & F_{2;32}^{332} \end{bmatrix} = \frac{1}{\sqrt{2}} \begin{bmatrix} 1 & -1 \\ -1 & 1 \end{bmatrix},$$

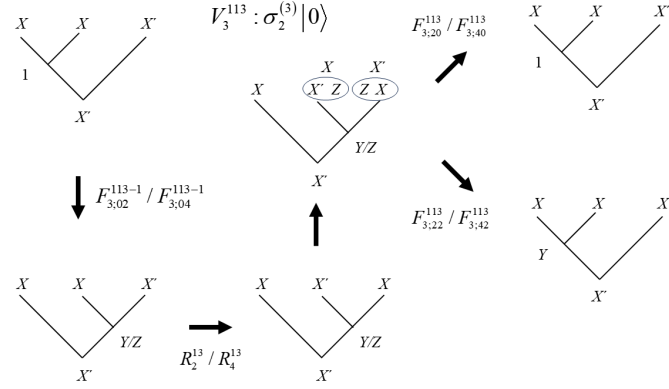
$$R_2^{13} = R_2^{31} = e^{i\frac{7\pi}{12}}, R_4^{13} = R_4^{31} = e^{i\frac{\pi}{4}}, R_0^{33} = e^{-i\frac{\pi}{4}}, R_2^{33} = e^{-i\frac{11\pi}{12}}.$$

Appendix C: The process of solving $\sigma_2^{(3)}$ and $\sigma_3^{(6)}$

Note that in the calculation processes, we ignore all F -matrices whose fusion result is vacuum, because it is always trivial.

We present an example of the braiding process for $\sigma_2^{(3)}/\sigma_3^{(6)}$ acting on $|0\rangle$ or $|00\rangle$ by the figure and other calculation results by formula:

Calculating $\sigma_2^{(3)}$ of the $\{V_3^{113}, V_3^{131}, V_1^{133}\}$ model:



$V_3^{113} :$

$$\begin{aligned}\sigma_2^{(3)} |0\rangle &= (F_{3;20}^{113} R_2^{13} F_{3;02}^{113-1} + F_{3;40}^{113} R_4^{13} F_{3;04}^{113-1}) |0\rangle + (F_{3;22}^{113} R_2^{13} F_{3;02}^{113-1} + F_{3;42}^{113} R_4^{13} F_{3;04}^{113-1}) |1\rangle \\ \sigma_2^{(3)} |1\rangle &= (F_{3;20}^{113} R_2^{13} F_{3;22}^{113-1} + F_{3;40}^{113} R_4^{13} F_{3;24}^{113-1}) |0\rangle + (F_{3;22}^{113} R_2^{13} F_{3;22}^{113-1} + F_{3;42}^{113} R_4^{13} F_{3;24}^{113-1}) |1\rangle\end{aligned}$$

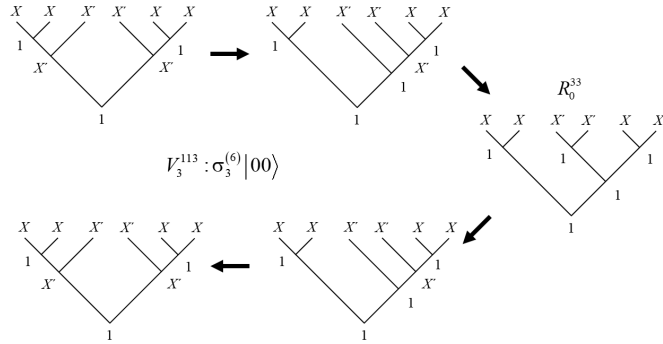
$V_3^{131} :$

$$\begin{aligned}\sigma_2^{(3)} |0\rangle &= (F_{3;22}^{131} R_2^{13} F_{1;22}^{131-1} + F_{1;42}^{131} R_4^{13} F_{1;24}^{131-1}) |0\rangle + (F_{1;24}^{131} R_2^{13} F_{1;22}^{131-1} + F_{1;44}^{131} R_4^{13} F_{1;24}^{131-1}) |1\rangle \\ \sigma_2^{(3)} |1\rangle &= (F_{1;22}^{131} R_2^{13} F_{1;42}^{131-1} + F_{1;42}^{131} R_4^{13} F_{1;44}^{131-1}) |0\rangle + (F_{1;24}^{131} R_2^{13} F_{1;42}^{131-1} + F_{1;44}^{131} R_4^{13} F_{1;44}^{131-1}) |1\rangle\end{aligned}$$

$V_1^{133} :$

$$\begin{aligned}\sigma_2^{(3)} |0\rangle &= (F_{1;02}^{133} R_0^{33} F_{1;20}^{133-1} + F_{1;22}^{133} R_2^{33} F_{1;22}^{133-1}) |0\rangle + (F_{1;04}^{133} R_0^{33} F_{1;20}^{133-1} + F_{1;24}^{133} R_2^{33} F_{1;22}^{133-1}) |1\rangle \\ \sigma_2^{(3)} |0\rangle &= (F_{1;02}^{133} R_0^{33} F_{1;40}^{133-1} + F_{1;22}^{133} R_2^{33} F_{1;42}^{133-1}) |0\rangle + (F_{1;04}^{133} R_0^{33} F_{1;40}^{133-1} + F_{1;24}^{133} R_2^{33} F_{1;42}^{133-1}) |1\rangle\end{aligned}$$

Calculating $\sigma_3^{(6)}$ of the $\{V_3^{113}, V_3^{131}, V_1^{133}\}$ model:



$V_3^{113} :$

$$\begin{aligned}\sigma_3^{(6)} |NC_1\rangle &= (F_{2;01}^{332-1} R_0^{33} F_{2;10}^{332} + F_{2;21}^{332-1} R_2^{33} F_{2;12}^{332}) |NC_1\rangle + (F_{2;03}^{332-1} R_2^{33} F_{2;10}^{332} + F_{2;23}^{332-1} R_0^{33} F_{2;12}^{332}) |11\rangle, \\ \sigma_3^{(6)} |00\rangle &= R_0^{33} |00\rangle, \sigma_3^{(6)} |01\rangle = R_2^{33} |01\rangle, \sigma_3^{(6)} |10\rangle = R_2^{33} |10\rangle, \\ \sigma_3^{(6)} |11\rangle &= (F_{2;01}^{332-1} R_0^{33} F_{2;30}^{332} + F_{2;21}^{332-1} R_2^{33} F_{2;32}^{332}) |NC_1\rangle + (F_{2;03}^{332-1} R_0^{33} F_{2;30}^{332} + F_{2;23}^{332-1} R_2^{33} F_{2;32}^{332}) |11\rangle,\end{aligned}$$

$V_3^{131} :$

$$\begin{aligned}\sigma_3^{(6)} |NC_1\rangle &= (F_{2;01}^{112-1} R_0^{11} F_{2;10}^{112} + F_{2;21}^{112-1} R_2^{11} F_{2;12}^{112}) |NC_1\rangle + (F_{2;03}^{112-1} R_0^{11} F_{2;10}^{112} + F_{2;23}^{112-1} R_2^{11} F_{2;12}^{112}) |00\rangle, \\ \sigma_3^{(6)} |NC_1\rangle &= (F_{2;01}^{112-1} R_0^{11} F_{2;30}^{112} + F_{2;21}^{112-1} R_2^{11} F_{2;32}^{112}) |NC_1\rangle + (F_{2;03}^{112-1} R_0^{11} F_{2;30}^{112} + F_{2;23}^{112-1} R_2^{11} F_{2;32}^{112}) |00\rangle, \\ \sigma_3^{(6)} |01\rangle &= R_2^{11} |01\rangle, \sigma_3^{(6)} |10\rangle = R_2^{11} |10\rangle, \sigma_3^{(6)} |11\rangle = R_0^{11} |11\rangle,\end{aligned}$$

$V_1^{133} :$

$$\begin{aligned}\sigma_3^{(6)} |NC_1\rangle &= (F_{2;03}^{332-1} R_0^{33} F_{2;30}^{332} + F_{2;23}^{332-1} R_2^{33} F_{2;32}^{332}) |NC_1\rangle + (F_{2;01}^{332-1} R_0^{33} F_{2;30}^{332} + F_{2;21}^{332-1} R_2^{33} F_{2;32}^{332}) |00\rangle, \\ \sigma_3^{(6)} |NC_1\rangle &= (F_{2;03}^{332-1} R_0^{33} F_{2;10}^{332} + F_{2;23}^{332-1} R_2^{33} F_{2;12}^{332}) |NC_1\rangle + (F_{2;01}^{332-1} R_0^{33} F_{2;10}^{332} + F_{2;21}^{332-1} R_2^{33} F_{2;12}^{332}) |00\rangle, \\ \sigma_3^{(6)} |01\rangle &= R_2^{33} |01\rangle, \sigma_3^{(6)} |10\rangle = R_2^{33} |10\rangle, \sigma_3^{(6)} |11\rangle = R_0^{33} |11\rangle,\end{aligned}$$

[1] J. M. Leinaas and J. Myrheim, *Il Nuovo Cimento B Series 11* **37**, 1 (2007).

[2] Jesper Jacobsen, Stephane, Ouvry, Vincent, Pasquier, Didina, Serban, Leticia, and C. J. C. courier, **51**, 52 (2011).

[3] S. Das Sarma, M. Freedman, and C. Nayak, *Physics Today* **59**, 32 (2006).

[4] C. Nayak, S. H. Simon, A. Stern, M. Freedman, and S. Das Sarma, *Reviews of Modern Physics* **80**, 1083 (2008).

[5] J. K. J. C. U. P. Pachos, (2012).

[6] C. Nayak and F. Wilczek, *Nuclear Physics B* **479**, 529 (1996).

[7] L. S. Georgiev, *Journal of Physics A: Mathematical and Theoretical* **42**, 10.1088/1751-8113/42/22/225203 (2009).

[8] J. K. Slingerland and F. A. Bais, *Nuclear Physics B* **612**, 229 (2001).

[9] S. Bravyi, *Physical Review A* **73**, 10.1103/PhysRevA.73.042313 (2006).

[10] O. Zilberberg, B. Braunecker, and D. Loss, *Physical Review A* **77**, 10.1103/PhysRevA.77.012327 (2008).

[11] M. H. Freedman, M. Larsen, and Z. Wang, *Communications in Mathematical Physics* **227**, 605 (2002).

[12] M. Burrello, H. Xu, G. Mussardo, and X. Wan, *Phys Rev Lett* **104**, 160502 (2010).

[13] C. M. Dawson and M. A. J. a. p. q.-p. Nielsen, (2005).

[14] E. Génetay Johansen and T. Simula, *PRX Quantum* **2**, 10.1103/PRXQuantum.2.010334 (2021).

[15] Y. H. Zhang, P. L. Zheng, Y. Zhang, and D. L. Deng, *Phys Rev Lett* **125**, 170501 (2020).

[16] R. B. McDonald and H. G. Katzgraber, *Physical Review B* **87**, 10.1103/PhysRevB.87.054414 (2013).

[17] L. Hormozi, G. Zikos, N. E. Bonesteel, and S. H. Simon, *Physical Review B* **75**, 10.1103/PhysRevB.75.165310 (2007).

[18] H. Xu and X. Wan, *Physical Review A* **78**, 10.1103/PhysRevA.78.042325 (2008).

[19] S. X. Cui, K. T. Tian, J. F. Vasquez, Z. Wang, and H. M. Wong, *Journal of Physics A: Mathematical and Theoretical* **52**, 10.1088/1751-8121/ab488e (2019).

[20] P. C. Burke, C. Aravanis, J. Aspman, J. Mareček, and J. Vala, *Physical Review A* **110**, 10.1103/PhysRevA.110.052616 (2024).

[21] A. Tounsi, N. E. Belaloui, M. M. Louamri, A. Benslama, and M. T. Rouabah, *Physical Review A* **110**, 10.1103/PhysRevA.110.012603 (2024).

[22] S. X. Cui, S.-M. Hong, and Z. Wang, *Quantum Information Processing* **14**, 2687 (2015).

[23] D. Naidu and E. C. Rowell, *Algebras and Representation Theory* **14**, 837 (2010).

[24] M. B. Hastings, C. Nayak, and Z. Wang, *Physical Review B* **87**, 10.1103/PhysRevB.87.165421 (2013).

[25] M. B. Hastings, C. Nayak, and Z. Wang, *Communications in Mathematical Physics* **330**, 45 (2014).

[26] S. X. Cui and Z. Wang, *Journal of Mathematical Physics* **56**, 10.1063/1.4914941 (2015).

[27] N. Read and E. Rezayi, *Physical Review B* **59**, 8084 (1999).

[28] M. Barkeshli and X. G. Wen, *Phys Rev Lett* **105**, 216804 (2010).

[29] D. J. Clarke, J. Alicea, and K. Shtengel, *Nat Commun* **4**, 1348 (2013).

[30] J. Fuchs, (1992).

[31] P. O. Boykin, in *IEEE*.

[32] M. Nagy and S. G. Akl, *International Journal of Parallel, Emergent and Distributed Systems* **21**, 1 (2006).

[33] C. I. Levaillant, (2015).

[34] B. Field and T. Simula, *Quantum Science and Technology* **3**, 10.1088/2058-9565/aacad2 (2018).

[35] N. E. Bonesteel, L. Hormozi, G. Zikos, and S. H. Simon, *Phys Rev Lett* **95**, 140503 (2005).

[36] H. Xu and J. M. Taylor, *Physical Review A* **84**, 10.1103/PhysRevA.84.012332 (2011).

[37] C. Levaillant, B. Bauer, M. Freedman, Z. Wang, and P. Bonderson, *Physical Review A* **92**, 10.1103/PhysRevA.92.012301 (2015).

[38] J. Long, X. Huang, J. Zhong, and L. Meng, arXiv:2501.01746 (2025).

[39] R. Raussendorf and J. Harrington, *Phys Rev Lett* **98**, 190504 (2007).

[40] A. G. Fowler, A. M. Stephens, and P. Groszkowski, *Physical Review A* **80**, 10.1103/PhysRevA.80.052312 (2009).

[41] A. G. Fowler, M. Mariantoni, J. M. Martinis, and A. N. Cleland, *Physical Review A* **86**, 10.1103/PhysRevA.86.032324 (2012).

[42] E. T. Campbell, B. M. Terhal, and C. Vuillot, *Nature* **549**, 172 (2017).

[43] P. Webster and S. D. Bartlett, *Physical Review A* **102**, 10.1103/PhysRevA.102.022403 (2020).

[44] S. Lomonaco, (2010).

[45] Y. J. Q. I. P. Makhlin, (2002).